Eur. Phys. J. A (2023) 59:187
https://doi.org/10.1140/epja/s10050-023-01099-0

THE EUROPEAN PHYSICAL JOURNAL A

Regular Article - Experimental Physics

Measurement of ^{58}co(*n*,*xp*) cross sections by a surrogate method

Ramandeep Gandhi[1,2,a], **S. Santra**[1,2,b], **P. C. Rout**[1,2], **A. Pal**[1,2], **A. Baishya**[1,2], **T. Santhosh**[1,2], **D. Chattopadhyay**[3], **K. Ramachandran**[1], **G. Mohanto**[1], **Jyoti Pandey**[4], **A. Diaz-Torres**[5], **R. Palit**[6]

[1] Nuclear Physics Division, Bhabha Atomic Research Centre, Mumbai 400085, India
[2] Homi Bhabha National Institute, Anushaktinagar, Mumbai 400094, India
[3] Faculty of Science and Technology (Physics), ICFAI University Tripura, Agartala 799210, India
[4] Inter University Accelerator Centre, P.O. Box 10502, New Delhi 110067, India
[5] Department of Physics, University of Surrey, Guildford, Surrey GU2 7XH, UK
[6] Department of Nuclear and Atomic Physics, Tata Institute of Fundamental Research, Mumbai 400005, India

Received: 2 April 2023 / Accepted: 2 August 2023
© The Author(s), under exclusive licence to Società Italiana di Fisica and Springer-Verlag GmbH Germany, part of Springer Nature 2023
Communicated by Aurora Tumino

Abstract The cross sections for ^{58}Co(*n*,*xp*) reactions have been determined in the equivalent neutron energy range of 11.7–16.8 MeV by employing the surrogate reaction ratio method and using the cross-section values for the reference reaction ^{60}Ni(*n*,*xp*) from the literature. The transfer reactions ^{57}Fe(^{6}Li,α) at $E_{\rm lab}$ = 37 MeV and ^{59}Co(^{6}Li,α) at $E_{\rm lab}$ = 33 MeV, are used to populate compound nuclei ^{59}Co* (surrogate of n+^{58}Co) and ^{61}Ni* (surrogate of n+^{60}Ni), respectively, at similar excitation energies. The evaporated protons at backward angles measured in coincidence with the projectile-like fragment alpha provide the proton decay probabilities of the compound nuclei. The cross sections estimated using the nuclear-reactions-model code TALYS-1.96 are consistent with the experimental ^{58}Co(*n*,*xp*) data for the entire neutron energy range. However, the predictions of the evaluated data libraries ENDF/B- VIII, JEFF-3.3, JENDL-5, ROSFOND-2010 and TENDL-2019 overestimate the present experimental data, indicating the necessity to improve the model parameters of the data libraries for this reaction.

1 Introduction

Improved and accurate nuclear data on neutron-induced reaction cross sections is of utmost importance for design and technology development of advanced reactors, such as accelerator driven systems and fusion reactors. The neutron energy spectra of these reactors exceed the typical limits of conventional fission reactors, resulting in more threshold reaction channels such as (*n*,*p*), (*n*,α), (*n*,*d*), (*n*,*np*), (*n*,2*n*), (*n*,3*n*) and (*n*,*n*α). In fusion reactors, high fluence of high energy neutrons produced via D + T reaction induce variety of reactions on the structural material (stainless steel). The reactions induced by neutrons that create gaseous elements, such as hydrogen and helium through (*n*,*xp*) and (*n*,*x*α) reactions are of critical importance, as they result in swelling and embrittlement of the reactor's structural material. Furthermore, these neutron impacts result in atomic displacements within the material, producing radiation defects that alter its physical properties. In addition to that these neutrons also alter the chemical composition of the structural material through transmutation reactions, resulting in noticeable changes in the material's structural and mechanical properties. ^{53}Mn($T_{1/2}$ = 3.74× 10^6 yr), ^{54}Mn($T_{1/2}$ = 312.3 d), ^{55}Fe($T_{1/2}$ = 2.73 yr), ^{60}Fe($T_{1/2}$ = 1.5 × 10^6 yr), ^{57}Co ($T_{1/2}$ = 271.79 d), ^{58}Co($T_{1/2}$ = 70.86 d), ^{60}Co($T_{1/2}$ = 5.27 yr), ^{59}Ni($T_{1/2}$ = 7.6 × 10^4 yr), ^{62}Cu($T_{1/2}$ = 9.67 min) and ^{63}Ni($T_{1/2}$ = 100.1 yr) are some of the radionuclei, that are produced through transmutation reactions on elements such as Mn, Fe, Ni, Cr, Cu, Zn, and Nb (initial composition of Stainless steel). To accurately predict the characteristics of the nuclear system and fully understand the neutronics of fusion reactors, experimental cross sections for (*n*,*xp*) and (*n*,*x*α) reactions involving these radionuclei is of great importance [1–5].

^{58}Co is among the dominant radionuclides produced during the fusion reactor operation, and is formed primarily through ^{58}Ni(*n*,*p*), ^{60}Ni(*n*,*d*)^{59}Co(*n*,2*n*), ^{60}Ni(*n*, 2*n*)^{59}Ni(*n*,*d*) and ^{60}Ni(*n*,*t*) reactions as depicted by routes in Fig. 1. The reactions ^{58}Ni(*n*,*p*) and ^{60}Ni(*n*,2*n*) have zero neutron threshold energies whereas, ^{59}Ni(*n*,*d*), ^{60}Ni(*n*,*d*), ^{59}Co(*n*,2*n*) and ^{60}Ni(*n*,*t*), have respective neutron threshold energy of 6.5, 7.4, 5.7 and 11.7 MeV.

[a] e-mail: ramangandhipu@gmail.com (corresponding author)
[b] e-mail: ssantra@barc.gov.in

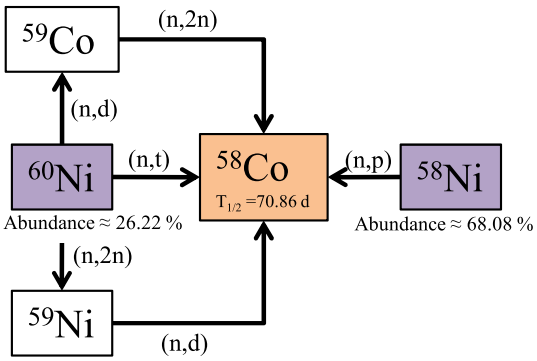

Fig. 1 Primary routes for production of ^{58}Co in a typical fusion reactor

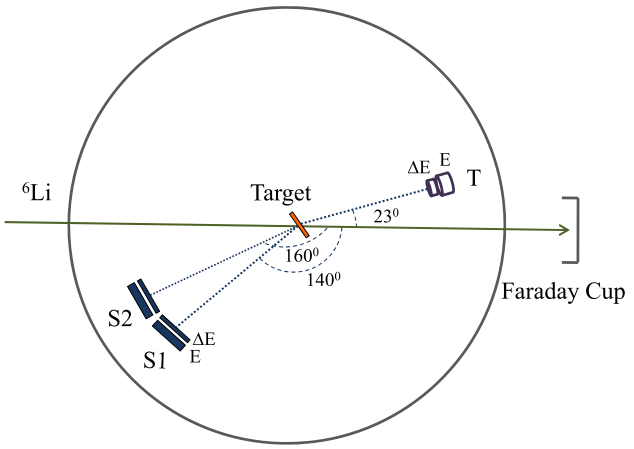

Fig. 2 Schematic experimental setup consisting of a Si surface barrier (SSB) detector telescope (T) positioned at 17 cm away from the target center to detect the projectile-like fragments (PLFs). S1 and S2 represent Si strip telescopes, each positioned at 17.6 cm from the target center for identification of the p, d, t, and α particles evaporated from the compound nucleus

As nickel makes up ≈10–14% of stainless steel's composition, the high energy neutron flux in a fusion reactor will result in a substantial increase in amount of ^{58}Co [6–8]. The exothermic reactions ^{58}Co(n,p) and ^{58}Co(n,α), with Q-values of 3.09 and 3.51 MeV, respectively, result in an enhanced yield of hydrogen and helium through (n,xp) and (n,$x\alpha$) reactions. So, it is important to measure the cross sections for ^{58}Co(n,xp) and ^{58}Co(n,$x\alpha$) reactions, for which data are not available in the database EXFOR [9] and the evaluated data libraries have large discrepancies among them for these reaction cross sections [10].

The isotope ^{58}Co is not available in nature, thus direct measurements of cross sections for ^{58}Co(n,xp) and ^{58}Co(n,$x\alpha$) reactions are challenging. Following our earlier works [5,11–13], we aim to determine ^{58}Co(n,xp) reaction cross sections by utilizing the surrogate reaction ratio method (SRM).

In the present work, the compound nuclei (CN) ^{59}Co* (surrogate of n+^{58}Co) and ^{61}Ni* (surrogate of n+^{60}Ni) were populated at matching excitation energies by the transfer reactions ^{57}Fe(^{6}Li,α) and ^{59}Co(^{6}Li,α), respectively. Using ^{60}Ni(n,xp) as the reference reaction, the cross sections for the desired reaction ^{58}Co(n,xp) are obtained by employing the SRM. The experimental setup and data analysis have been described in detail in Sect. 2. The results and discussions can be found in Sect. 3, and the summary and conclusions are presented in Sect. 4.

2 Experimental details and data analysis

The experiment was performed by bombarding ^{6}Li beams of energies $E_{\rm lab}$ = 37 and 33 MeV, on freshly prepared self-supporting targets of ^{57}Fe (enrichment ≈ 95%, thickness ≈ 850 μg/cm^2) and ^{59}Co (abundance ≈ 100%, thickness ≈ 500 μg/cm^2), respectively at BARC-TIFR Pelletron Linac Accelerator Facility, Mumbai.

Figure 2 shows the schematic representation of the experimental configuration, where PLFs were identified by employing a silicon surface barrier (SSB) telescope T comprising of one ΔE detector having thickness of ≈ 150 μm and one E detector having thickness of ≈ 1 mm. The telescope was placed at 23° (around grazing angle) with respect to the direction of beam. Energy calibrations of both the detectors were performed using ^{229}Th alpha source, emitting alphas having five different known energies in the range of 4.6–8.7 MeV. After calibrating ΔE and E detectors separately, one can find the incident energy ($E_{\rm total}$) of the PLFs by adding energy deposited in the two detectors, on event by event basis. Figure 3a shows the energy calibrated two dimensional correlation plot of ΔE versus $E_{\rm total}$ which is clearly distinguishing the different PLFs, i.e., proton (p), deuteron (d), triton (t), and α particles. By identifying alpha band from the above plot, one can confirm the formation of the CN ^{59}Co* and ^{61}Ni* populated in the transfer reactions ^{57}Fe(^{6}Li,α) and ^{59}Co(^{6}Li,α), respectively. The SSB telescope had an energy resolution of ≈ 160 keV.

To detect the charge particles (such as p, d, t, and α) evaporated from CN of interest (^{59}Co* and ^{61}Ni*), two large area Silicon strip detector telescopes (S1 and S2) were placed at backward angles 140° and 160°. Each strip telescope, having total active area of 50 × 50 mm, is made of 16 segmented ΔE (thickness ≈ 55 μm) and 16 segmented E detectors (thickness ≈ 1500 μm). Each strip telescope was placed at a distance of 17 cm from the target centre. Energy calibrations were performed using the same method discussed earlier. A typical two dimensional ΔE versus $E_{\rm total}$ correlation plot corresponding to one of the $\Delta E - E$ strip combinations of the S1 telescope is shown in Fig. 3b, which clearly identifies different isotopes with $z = 1$ and $z = 2$. The energy reso-

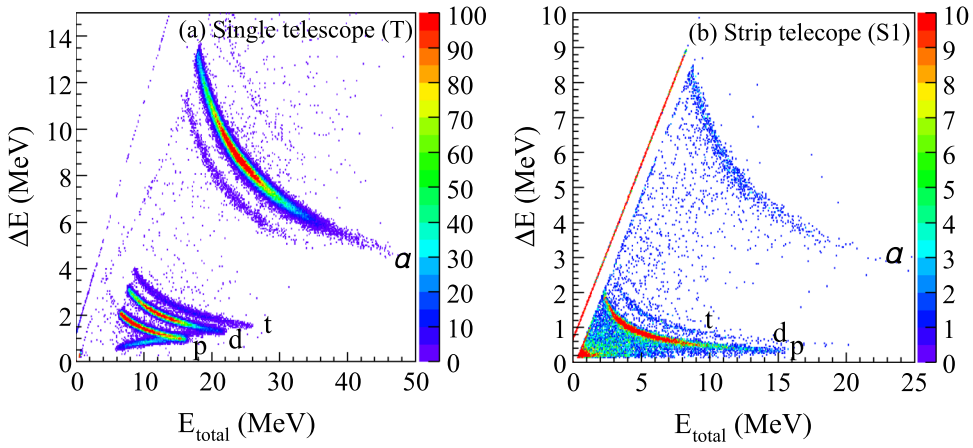

Fig. 3 **A** Typical energy calibrated 2D spectra of ΔE versus E_{total} (total energy) for outgoing particles in ^{6}Li + ^{57}Fe reaction at E_{lab}= 37 MeV, acquired using (**a**) Si surface barrier detector telescope (T) placed at 23° and (**b**) one of the 16 $\Delta E - E$ strip combinations of Si strip detector telescope S1

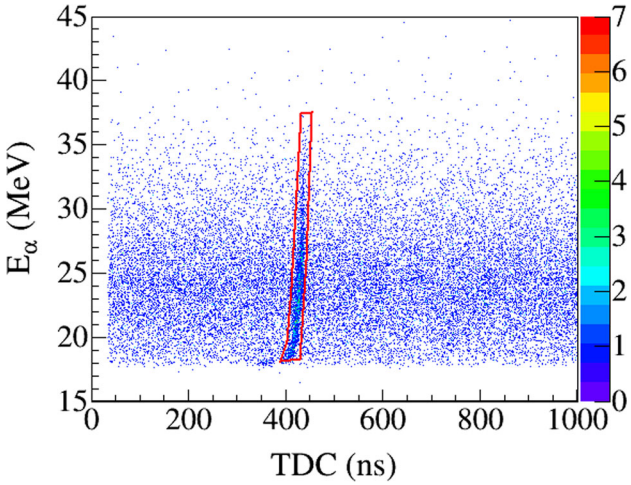

Fig. 4 For ^{6}Li + ^{57}Fe reaction at E_{lab} = 37 MeV, a two-dimensional plot of the α-particle energy (E_α) detected in the telescope T versus time correlation between the α particles detected in the telescope T and the protons detected in the telescope S1

lution of a ΔE or E strip detector was found to be $\approx$ 100 keV.

A Time to Digital Converter (TDC) was used to register the time correlations between the particles detected in the telescope T and the particles detected in the telescope S1 or S2. A sharp peak in the TDC spectra was observed which was further used to obtain the real coincidence events between the alpha detected in T and proton detected in S1 and/or S2. A two-dimensional plot of the α-particle energy (E_α) detected in telescope T versus TDC output gated with alpha band from T1 and proton band from S1 is shown in Fig. 4 for ^{6}Li + ^{57}Fe system at E_{lab} = 37 MeV. The intense band as shown by a red contour in the above plot corresponds to the coincidence events of our interest. However, the contribution from random background estimated from the remaining region of Fig. 4 has been taken into account to obtain the real coincidence events.

The excitation energy spectra of target-like composite nuclei ^{59}Co* and ^{61}Ni* formed in the transfer reactions ^{57}Fe(^{6}Li,α) and ^{59}Co(^{6}Li,α), respectively, are obtained through "event-by-event analysis"using the 2-body kinematics. The excitation energy spectra recorded in singles as well as in coincidence with the evaporated proton corresponding to the ^{59}Co* are shown in Fig. 5(a, c), and those corresponding to ^{61}Ni* are shown in Fig. 5(b, d), respectively. One can notice that there are significant overlaps in the excitation energy spectra corresponding to the two compound nuclei.

To confirm that the protons detected in the strip telescopes in coincidence with the α detected in T, are actually evaporated at back angles from the nucleus ^{59}Co*, the proton energy spectra are compared with the ones obtained from ^{59}Co* formed at $E^* = 25$ MeV using the statistical model code PACE4 [14] and shown in Fig. 6. It can be observed that the emitted proton spectrum and PACE4 predictions are in good agreement with each other, thus confirming proton evaporation from the compound system ^{59}Co*. Furthermore, angular distribution of those protons is found to be isotropic in the center of mass in the angular range ($\approx$ 130°–170°) spanned by S1 and S2, which is another affirmative sign of evaporation. The similar comparison has been made for the other nuclei ^{61}Ni*, but not shown here.

Now, the following expression is used to obtain the proton decay (particle evaporation) probabilities from the compound systems ^{59}Co* and ^{61}Ni* produced in their respective transfer reactions, in steps of 1.0-MeV excitation energy bin.

$$P_p^{CN}(E^*) = \frac{N_{\alpha,p}(E^*)}{\epsilon N_\alpha(E^*)}. \quad (1)$$

Here, N_α represents the singles counts (α-PLF) and $N_{\alpha,p}$ represents the counts of α-PLF which are coincidence with the evaporated p, both acquired at the same excitation energy (E^*). ϵ is the efficiency of detecting evaporated protons in coincidence with the PLFs. The ratios of $N_{\alpha,p}$ to N_α obtained as a function of E^* for compound systems ^{59}Co* and ^{61}Ni* are presented in Fig. 7.

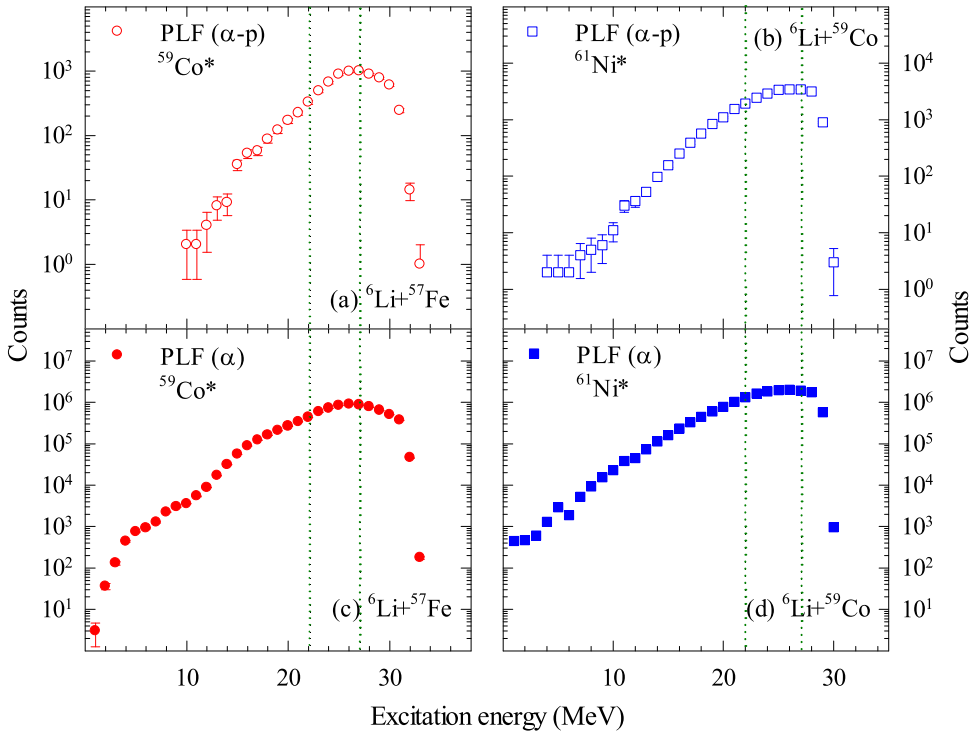

Fig. 5 Excitation energy spectra corresponding to the target-like compound nuclei ^{59}Co* and ^{61}Ni* formed in ^{6}Li + ^{57}Fe and ^{6}Li + ^{59}Co reactions, respectively, corresponding to α-PLF with (**a**, **b**) and without (**c**, **d**) coincidence with evaporated protons. The desired cross sections are determined for matching excitation energy range within the two dotted lines

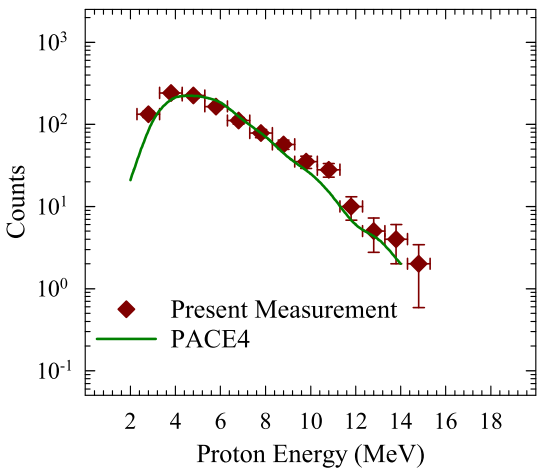

Fig. 6 The energy spectrum of protons (in coincidence with α-PLF) emitted from compound nucleus ^{59}Co* at excitation energy $E^* \approx 25$ MeV, corresponding to ^{6}Li + ^{57}Fe reaction at $E_{\rm lab}$ = 37 MeV. Continuous line represents the prediction of the same by PACE4 [14] after normalization

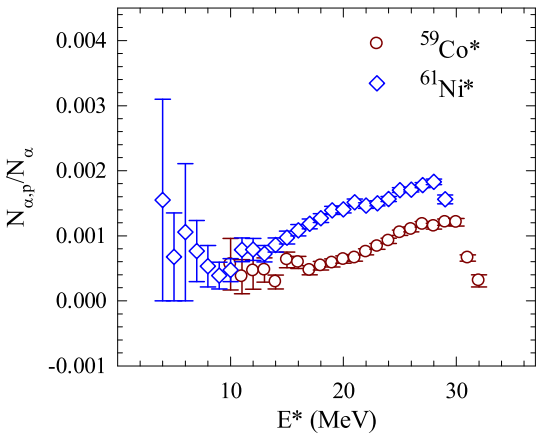

Fig. 7 $N_{\alpha,p}/N_{\alpha}$, the ratio of α-PLF counts in coincidence with the evaporated protons to the singles α-PLF counts as a function of E^*, for compound systems ^{59}Co* and ^{61}Ni* formed in the reactions ^{57}Fe(^{6}Li,α) and ^{59}Co(^{6}Li,α), respectively

Following the description given in Refs. [5,11–13], the cross sections for the desired reaction ($\sigma^{^{58}Co(n,xp)}$) are determined using the following expression:

$$\frac{\sigma^{^{58}Co(n,xp)}(E^*)}{\sigma^{^{60}Ni(n,xp)}(E^*)} = \frac{\sigma^{CN}_{n+^{58}Co}(E^*)}{\sigma^{CN}_{n+^{60}Ni}(E^*)} \frac{\mathrm{P}^{^{59}Co}_{p}(E^*)}{\mathrm{P}^{^{61}Ni}_{p}(E^*)} \qquad (2)$$

The experiment for both the desired and the reference surrogate reactions was performed using the same experimental geometry/setup which make the ratio of efficiency corresponding to the desired reaction to that of the reference reaction equal to 1 in Eq. (2). Therefore, while taking the ratio of $P_p^{^{59}Co^*}(E^*)$ to $P_p^{^{61}Ni^*}(E^*)$ in Eq. (2) one can omit the ϵ term. The cross sections for neutron-induced compound nucleus formation i.e., $\sigma^{CN}_{n+^{58}Co}$ and $\sigma^{CN}_{n+^{60}Ni}$ are calculated for E^* = 22–27 MeV, using the nuclear-reactions-model code TALYS-1.96 [15]. In Ref. [12], it has been found that the direct measurements on ^{60}Ni(n,xp) cross sections are quite close to the evaluations by JENDL-4.0 [16]. Therefore,

the JENDL-4.0 evaluated cross sections were used as reference for the present work.

Now using (1) the cross sections for ^{60}Ni(n,xp) reaction, $\sigma^{^{60}Ni(n,xp)}$, (2) the calculated neutron-induced compound nucleus formation cross sections, $\sigma^{CN}_{n+^{58}Co}(E^*)$ and $\sigma^{CN}_{n+^{60}Ni}(E^*)$, obtained from the TALYS-1.96 code and (3) the measured proton decay probabilities for compound systems, $P_p^{^{59}Co^*}(E^*)$ and $P_p^{^{61}Ni^*}(E^*)$, obtained from Eq. (1), the desired cross sections for the ^{58}Co(n,xp) reaction are determined at same excitation energy with the help of Eq. (2). The desired reaction cross sections have been obtained in steps of 1 MeV of excitation energy bin in the range of E^* = 22–27 MeV.

Using the following relation, this E^* range is later converted into equivalent neutron energy range of E_n = 11.7–16.8 MeV.

$$E_n = \frac{A+1}{A}(E^* - S_n) \tag{3}$$

Here, $A + 1$ (= 59) and S_n (= 10.454 MeV) are the mass and the neutron separation energy of the compound nucleus ^{59}Co, respectively.

In Ref. [17], Chiba et al. have investigated the applicability of the SRM to determine n-induced fission (or capture) cross sections, where they studied the branching ratio to the fission (or capture), up to $J^\pi = (\frac{21}{2})^\pm$ and neutron energy of 5 MeV. It was found that by satisfying three conditions given in the paper, the SRM can be employed to determine neutron fission and capture cross sections to the accuracy of order of J^π-by-J^π convergence of the branching ratios (defined in the paper). Following Ref. [17], we have also investigated the applicability of the SRM to determine the desired (n,xp) cross sections and, studied the proton decay branching ratios, up to $J^\pi = (9)^\pm$ and excitation energies of our interest. We have found that the SRM can be used to determine the desired (n,xp) cross sections with the accuracy of the order of J^π-by-J^π convergence (as discussed in the following subsection) subjected to the fulfillment of following three conditions. The three conditions to be satisfied are: (1) weak Weisskopf–Ewing condition which requires J^π-by-J^π convergence of the branching ratios in the two surrogate reactions, (2) the spin distributions in two compound nuclei populated by the two surrogate reactions used in the SRM are almost equivalent, and (3) the representative spin values populated in both the surrogate reactions are not much larger than $9\hbar$.

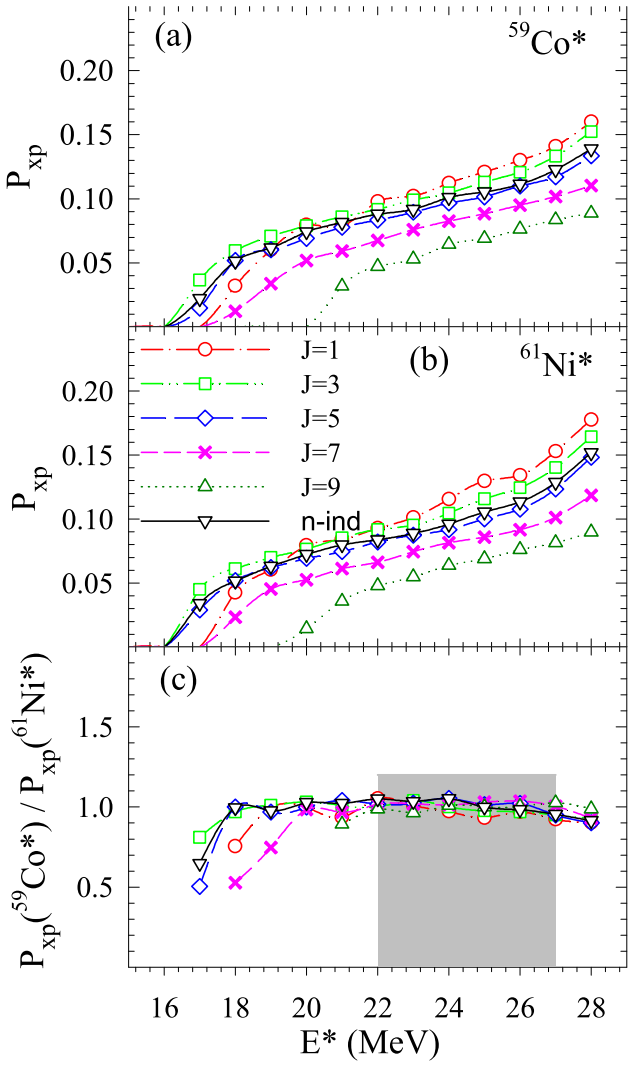

Fig. 8 **a** The proton decay probabilities (branching ratios) P_{xp} of different spin states (J) for the compound nucleus ^{59}Co* produced in the surrogate reaction ^{57}Fe(^{6}Li,α) along with P_{xp} for same CN produced in n-induced reaction n+^{58}Co, as a function of excitation energy (E*), **b** Same as (**a**) but for CN ^{61}Ni* produced in the surrogate reaction ^{59}Co(^{6}Li,α) and n-induced reaction n+^{60}Ni, **c** ratio of P$_{xp}$ of two CN ^{59}Co* and ^{61}Ni* i.e $P_{xp}(^{59}\text{Co}^*)/P_{xp}(^{61}\text{Ni}^*)$ of various spin (J) states produced in surrogate reactions along with $P_{xp}(^{59}\text{Co}^*)/P_{xp}(^{61}\text{Ni}^*)$ for CN produced in the the n-induced reactions, as a function of E^*. Excitation energy region within the shaded gray band is of our interest for determining the desired cross sections

2.1 J^π-by-J^π convergence

Statistical model calculations are carried out to determine the proton decay branching ratios (proton decay probabilities) P_{xp} of individual spin (J) states of the compound

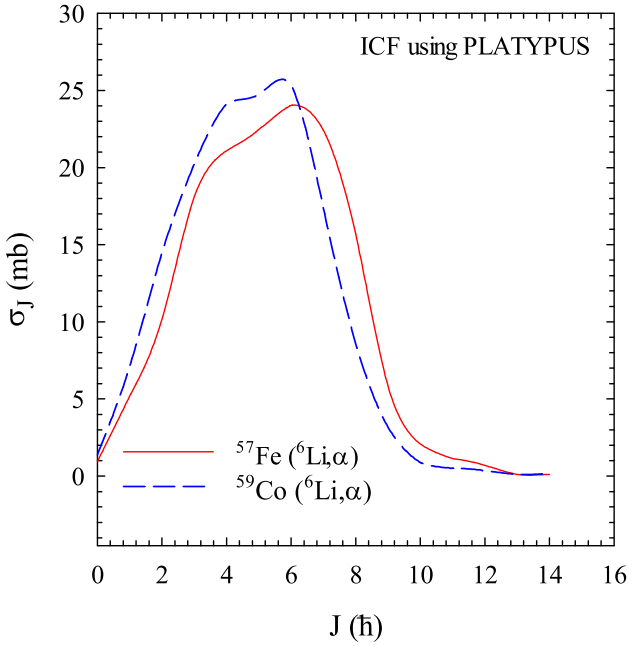

Fig. 9 Calculations using PLATYPUS (a three-body classical dynamical model code) to compute the incomplete fusion/transfer cross sections for the reactions ^{57}Fe(^{6}Li,α)^{59}Co* at E_{beam} = 37 MeV (solid line) and ^{59}Co(^{6}Li,α)^{61}Ni* at E_{beam} = 33 MeV (dashed line)

nuclei ^{59}Co* and ^{61}Ni* (the CN populated in corresponding surrogate reactions ^{57}Fe(^{6}Li,α) and ^{59}Co(^{6}Li, α), respectively), using the code PACE4. The calculations are performed up to J = 9 for excitation energies ranging from 15 to 28 MeV, as shown by colored dashed/dotted lines in Fig. 8(a, b). In the excitation energy range of our interest (E^* = 22–27 MeV), the P_{xp} shows similar behaviour for both the parity states ($\pm$) of the same J-value. Hence, only J-dependence of P_{xp} is considered in the present study. The black solid curves (n-induced curve) in these figures represent the proton decay branching ratios of the CN ^{59}Co* and ^{61}Ni* produced in the respective neutron-induced reactions n+^{58}Co and n+^{60}Ni, calculated using the code PACE4. The results indicate that proton decay probabilities (P_{xp}) depend significantly on J-state of the decaying compound nucleus (^{59}Co* and ^{61}Ni*), indicating that the standard Weisskopf–Ewing approximation (which assumes independence of decay branching ratios from spin-parity states) is not fulfilled for present systems. However, the ratio of the two decay probabilities ($P_{xp}(^{59}\text{Co}^*)/P_{xp}(^{61}\text{Ni}^*)$) for each J state (colored dashed/dotted lines in Fig. 8c) converge among themselves and to that of neutron induced reaction (black solid line in Fig. 8c) with an uncertainty of 5.5–8.7% for excitation energy range E^* = 22–27 MeV (gray band in Fig. 8c), indicating the weak J dependence of the ratio. But, for the excitation energies lower than 22 MeV (E_n = 11.7 MeV) J-curves diverge substantially (up to 47%) from n-induced curve, implying that the weak Weisskopf–Ewing condition may not be fulfilled for E^* lower than 22 MeV. Hence, first condition i.e., weak Weisskopf–Ewing approximation which requires the "J^π-by-J^π convergence"of the branching ratios, is satisfied for E^* = 22–27 MeV.

2.2 Equivalence of spin distribution

The spin distributions (σ_J vs J) of the ^{59}Co* and ^{61}Ni* compound nuclei formed in the surrogate reactions ^{57}Fe(^{6}Li,α) and ^{59}Co(^{6}Li,α), at respective beam energies of 37 and 33 MeV, are calculated using PLATYPUS [18–20], a three-body classical dynamical model code. The parameters for the interaction potentials of projectile-target (^{6}Li+^{57}Fe/^{59}Co) and of fragment-target (α+^{57}Fe/^{59}Co) are taken from the global Broglia–Winther parametrization [21], while the parameters for the fragment–fragment (d+α) interaction potentials are

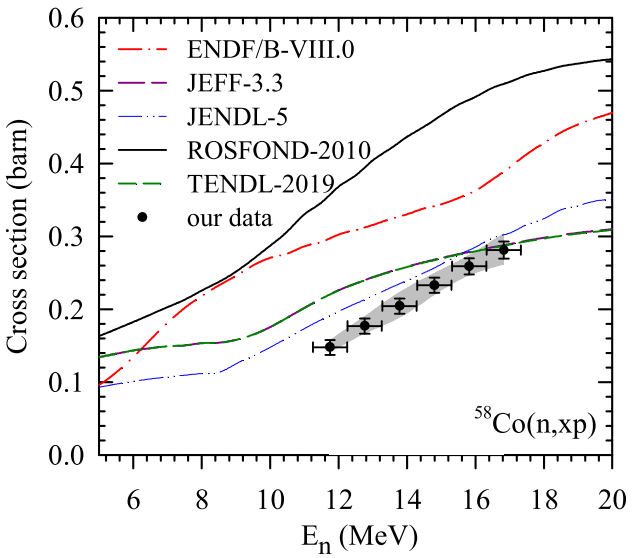

Fig. 10 The cross sections for ^{58}Co(n,xp) reactions, determined by SRM, as a function of equivalent or incident neutron energy (E_n), represented by filled circles, are compared to the predictions from different evaluated nuclear data libraries. The gray shaded area surrounding experimental data points indicates additional uncertainty in measured cross sections due to systematic uncertainties inherent to application of SRM (see text)

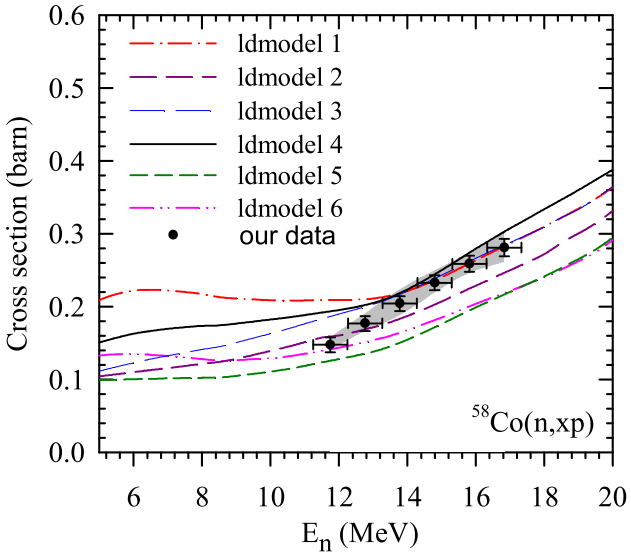

Fig. 11 The measured cross section for ^{58}Co(n,xp) reactions are compared to the predictions from the TALYS-1.96 code using various level density models (see text)

taken from Ref. [22]. The input parameters determining the probability density of two-body projectile ^{6}Li in ground state is taken from Ref. [23]. The calculated spin distributions (σ_J vs J) of both the populated compound nuclei are found to be very similar, as presented in Fig. 9. This demonstrates the equivalence of the spin distributions of the two compound nuclei populated in respective surrogate reactions of interest.

2.3 Spin population in the surrogate reactions

The spin distribution presented in Fig. 9 is used to deduce the representative spin (J) values populated in the compound nuclei ^{59}Co* and ^{61}Ni* by their respective surrogate reactions. Clearly, the J-values populated by both the surrogate reactions used in the present study are not much larger than $9\hbar$.

Therefore, all three conditions are fulfilled for the present systems, implying that the SRM can be reliably employed to deduce the reaction cross sections of our interest, for E^* range of 22–27 MeV, with a theoretical systematic uncertainty (accuracy) of 5.5–8.7%.

3 Results and discussions

The ^{58}Co(n,xp) reaction cross sections are determined using Eq. (2) following the SRM methodology as described above and the results are presented as filled circles in Figs. 10 and 11. In these figures, the cross section error bars represent statistical errors, whereas equivalent neutron energy error bars correspond to the width of 1.0-MeV energy bins. The numerical values for various quantities used in Eq. (2) to determine ^{58}Co(n,xp) reaction cross sections and results are given in Table 1. The experimental systematic uncertainties in the present work are considerably lower than the error bars shown in these figures. The SRM has the advantage of significantly reducing most of the systematic errors on cross sections that may arise from detector efficiency, flux normalisation, etc. The systematic errors in equivalent neutron energies caused by uncertainties in target thickness, beam energy, kinematic broadening, etc. are estimated to be considerably smaller than the energy bin width [5,24].

Deviations in J^π-by-J^π convergence of branching ratios described in Sect. 2.1, are the main source of theoretical systematic uncertainties in application of the SRM to determine the ^{58}Co(n,xp) reaction cross sections. This deviation is evaluated at each E^* bin, and found to be 5.5–8.7% for the E^* range of 22–27 MeV (i.e., equivalent neutron energy range E_n = 11.7–16.8 MeV). The gray shaded areas surrounding the experimental data points in Figs. 10 and 11, depict the evaluated theoretical systematic uncertainties.

The measured ^{58}Co(n,xp) cross sections are compared with the predictions of evaluated nuclear data libraries: ENDF/B- VIII, JEFF-3.3, JENDL-5, ROSFOND-2010 and TENDL-2019, as shown in Fig. 10. The evaluated ^{58}Co(n,xp) cross sections are obtained by adding cross sections for proton emitting ^{58}Co(n,p), ^{58}Co(n,np) and ^{58}Co(n,2p) reaction channels which are possible sources for proton emission contributing in the measured excitation energy region. The evaluated ^{58}Co(n,xp) cross sections are observed to be consistently higher than the measured ones in the entire equivalent neutron energy range of interest.

Statistical model calculations (Hauser–Feshbach statistical model [25]) are performed to quantify the cross sections for the ^{58}Co(n,xp) reaction using the TALYS-1.96 code. Nuclear masses, ground-state deformations, γ-ray strength functions, transmission coefficients and nuclear level densities (NLD) of nuclides involved, which are used as default input to the TALYS-1.96, are taken from the latest Reference Input Parameter Library RIPL-3 [26]. The transmission coefficients used in present calculations, are calculated by global parameterisation of optical model potentials for neutron and proton proposed by Koning and Delaroche [27]. The discrete levels of all the nuclei involved have been taken from the level density estimates using the option "disctable 3". In the TALYS-1.96 version, there are six different options for determining the level densities of the nuclei involved in a reaction, each corresponding to a different level-density model. The first three options "ldmodel 1, 2 and 3"derive level density from three phenomenological analytical expressions i.e., (i) constant temperature + Fermi gas model [28], (ii) back-shifted Fermi gas model [29] and (iii) Generalized superfluid model [30], respectively. Whereas, the other three options take tabulated level densities derived from microscopic mod-

Table 1 The neutron-induced compound nuclear formation cross sections for CN ^{59}Co* and ^{61}Ni* ($\sigma^{CN}_{n+^{58}Co}$ and $\sigma^{CN}_{n+^{60}Ni}$) calculated using TALYS-1.96 code, the experimental proton decay probabilities $P_p(E^*)$ of the corresponding compound nuclei (CN) ^{59}Co* and ^{61}Ni* produced via transfer reactions ^{57}Fe(^{6}Li,α) and ^{59}Co(^{6}Li,α), the cross section values for the reference reaction ^{60}Ni(n,xp), the cross sections for desired reaction ^{58}Co(n,xp) determined using Eq. (2), and (v) the equivalent neutron energy (En) corresponding to excitation energy (E^*) of the compound nucleus ^{59}Co* deduced using Eq. (3)

E^* (MeV)	$\sigma^{CN}_{n+^{58}Co}$ (mb)	$\sigma^{CN}_{n+^{60}Ni}$ (mb)	$P_p^{^{59}Co}(E^*)$	$P_p^{^{61}Ni}(E^*)$	$\sigma^{^{60}Ni(n,xp)}$ (b)	$\sigma^{^{58}Co(n,xp)}$ (b)	E_n (MeV)
22	968	1037	0.00075	0.00146	0.31	0.15±0.010	11.7±0.5
23	906	982	0.00084	0.00150	0.34	0.18±0.010	12.8±0.5
24	843	928	0.00092	0.00156	0.38	0.20±0.010	13.8±0.5
25	785	876	0.00105	0.00170	0.42	0.23±0.010	14.8±0.5
26	731	826	0.00110	0.00171	0.46	0.26±0.011	15.8±0.5
27	680	777	0.00118	0.00178	0.49	0.28±0.012	16.8±0.5

els, i.e., "ldmodel 4, 5 and 6"correspond to the microscopic level densities obtained from (i) Goriely's tables [31], (ii) Hilaire's combinatorial tables [32] and (iii) Temperature-dependent Gogny–Hartree–Fock–Bogoliubov level densities from numerical tables [33]. The calculated cross sections for ^{58}Co(n,xp) reaction using these ldmodel options in TALYS-1.96 are shown in Fig. 11. It is observed that the calculations using "ldmodel 1 and 3"options compare best with the measured data for equivalent neutron energy range of our interest.

4 Summary and conclusion

In summary, we have employed the surrogate reaction ratio method to determine the ^{58}Co(n,xp) reaction cross sections. Here, the ^{59}Co* and ^{61}Ni* nuclei, which are desired to be formed in respective reactions: n + ^{58}Co and n + ^{60}Ni, are instead populated using two surrogate reactions: ^{57}Fe(^{6}Li,α)^{59}Co* and ^{59}Co(^{6}Li,α)^{61}Ni*, respectively at similar excitation energies. Thereafter, the ratio of proton decay probabilities from those two compound nuclei were measured in the excitation energy range of 22–27 MeV. The ratio of formation cross sections of those two nuclei in the two n-induced reaction was calculated using the code TALYS-1.96. Finally, the cross sections for ^{58}Co(n,xp) reaction have been determined using ^{60}Ni(n,xp) cross sections as the reference, in the equivalent neutron energy of 11.7–16.8 MeV. The experimental results of the ^{58}Co(n,xp) cross sections are compared with the predictions from nuclear-reactions-model code TALYS-1.96 and the predictions from the evaluated data libraries: ENDF/B- VIII, JEFF-3.3, JENDL-5, ROSFOND-2010 and TENDL-2019. The TALYS-1.96 predictions compare well with the measured ^{58}Co(n,xp) cross sections, whereas predictions of all of the above evaluations are found to be higher. The observed differences between the measured ^{58}Co(n,xp) reaction cross sections and predictions from the evaluated data libraries: ENDF/B- VIII, JEFF-3.3, JENDL-5, ROSFOND-2010 and TENDL-2019, indicate the need to revisit and improve the model parameters of these evaluations for this reaction.

Acknowledgements We express our gratitude to the operating personnel of the BARC-TIFR Pelletron Accelerator for ensuring the seamless operation of the accelerator during the experiment. Our appreciation goes to the Department of Atomic Energy, Government of India, for their support under the Project Identification No. RTI 4002. R.G. extend sincere thanks to Gaurishankar and Maheshwari for their invaluable guidance and support. Additionally, A.D-T's work is supported by the STFC Consolidated Grant No. ST/P005314/1.

Data Availability Statement This manuscript has no associated data or the data will not be deposited. [Authors' comment: There are no associated data available.]

References

1. Report summary of European facility for innovative reactor and transmutation neutron data (2013), Belgium, id:211499. https://cordis.europa.eu/project/rcn/88553/reporting/en
2. H. Iida, V. Khripunov, L. Petrizzi, G. Federici, Tech. Rep. G 73 DDD 2W 0.2, Nuclear Analysis Group, ITER Naka & Garching Joint Work Sites (2004)
3. M.R. Gilbert, S. Dudarev, S. Zheng, L.W. Packer, J. Sublet, Nucl. Fusion **52**, 083019 (2012)
4. S. Fetter, E.T. Cheng, F.M. Mann, Fusion Eng. Des. **6**, 123–130 (1988)
5. R. Gandhi et al., Phys. Rev. C **106**, 034609 (2022)
6. R.A. Forrest, Fusion Eng. Des. **81**, 2143 (2006)
7. R.A. Forrest, A. Tabasso, C. Danani, S. Jakhar, A.K. Shaw, *Handbook of Activation Data Calculated Using EASY-2007* (EURATOM / UKAEA Fusion Association, Culham Science Centre, Abingdon, UK, 2009), p.184
8. J.M.A. Plompen, D. Smith, P. Reimer, S. Qaim, V. Semkova, F. Cserpák, V. Avrigeanu, S. Sudar, J. Nucl. Sci. Technol. **39**, 192 (2002)
9. EXFOR Data Library. https://www-nds.iaea.org/exfor/exfor.htm
10. ENDF Data Library. https://www-nds.iaea.org/exfor/endf.htm
11. B. Pandey et al., Phys. Rev. C **93**, 021602(R) (2016)
12. J. Pandey et al., Phys. Rev. C **99**, 014611 (2019)
13. R. Gandhi et al., Phys. Rev. C **100**, 054613 (2019)
14. A. Gavron, Phys. Rev. C **21**, 230 (1980)

15. A.J. Koning, S. Hilaire, M.C. Duijvestijn, TALYS-1.0. *Proceedings of the International Conference on Nuclear Data for Science and Technology*, April 22–27, 2007, ed. by Nice, France, O. Bersillon, F. Gunsing, E. Bauge, R. Jacqmin, and S. Leray (EDP Sciences, 2008), pp. 211–214
16. K. Shibata et al., J. Nucl. Sci. Technol. **48**, 1 (2011)
17. S. Chiba, O. Iwamoto, Phys. Rev. C **81**, 044604 (2010)
18. A. Diaz-Torres, Comput. Phys. Commun. **182**, 1100 (2011)
19. A. Diaz-Torres, D.J. Hinde, J.A. Tostevin, M. Dasgupta, L.R. Gasques, Phys. Rev. Lett. **98**, 152701 (2007)
20. A. Diaz-Torres, J. Phys. G Nucl. Part. Phys. **37**, 075109 (2010)
21. W. Reisdorf, J. Phys. G Nucl. Part. Phys. **20**, 1297 (1994)
22. A. Diaz-Torres, I.J. Thompson, C. Beck, Phys. Rev. C **68**, 044607 (2003)
23. A. Diaz-Torres, D. Quraishi, Phys. Rev. C **97**, 024611 (2018)
24. J.E. Escher, J.T. Burke, F.S. Dietrich, N.D. Scielzo, I.J. Thompson, W. Younes, Rev. Mod. Phys. **84**, 353 (2012)
25. W. Hauser, H. Feshbach, Phys. Rev. C **87**, 366 (1952)
26. R. Capote et al., Nucl. Data Sheets **110**, 3107 (2009)
27. A.J. Koning, J.P. Delaroche, Nucl. Phys. A **713**, 231 (2003)
28. A. Gilbert, A.G.W. Cameron, Can. J. Phys. **43**, 1446 (1965)
29. W. Dilg, W. Schantl, H. Vonach, M. Uhl, Nucl. Phys. A **217**, 269 (1973)
30. A.V. Ignatyuk, J.L. Weil, S. Raman, S. Kahane, Phys. Rev. C **47**, 1504 (1993)
31. S. Goriely, F. Tondeur, J. Pearson, Atom. Data Nucl. Data Tables **77**, 311 (2001)
32. S. Goriely, S. Hilaire, A.J. Koning, Phys. Rev. C **78**, 064307 (2008)
33. S. Hilaire, M. Girod, S. Goriely, A.J. Koning, Phys. Rev. C **86**, 064317 (2012)

Springer Nature or its licensor (e.g. a society or other partner) holds exclusive rights to this article under a publishing agreement with the author(s) or other rightsholder(s); author self-archiving of the accepted manuscript version of this article is solely governed by the terms of such publishing agreement and applicable law.